Renewable Energy 180 (2021) 14–29

Contents lists available at ScienceDirect

Renewable Energy

journal homepage: www.elsevier.com/locate/renene

Off-design performance analysis of combined CSP power and direct oxy-combustion supercritical carbon dioxide cycles

Ahmad K. Sleiti , Wahib A. Al-Ammari *

Department of Mechanical & Industrial Engineering, College of Engineering, Qatar University, Doha, 2713, Qatar

ARTICLE INFO

Article history:
Received 20 May 2021
Received in revised form
10 August 2021
Accepted 12 August 2021
Available online 19 August 2021

Keywords:
Off-design performance
Solar power tower
Supercritical CO_2 power cycle
Direct oxy-combustion

ABSTRACT

The solar power tower (SPT) has the potential to achieve high efficiency and large-scale power production due to its high achievable temperatures. However, thermal energy storage (TES) is required to solve the intermittency problem of the solar energy and to provide a dispatchable power production according to the power demand profile. Critical technical problems still exist in the TES systems including the high-temperature corrosion, expensive materials, temperature swing, and large size. Therefore, newly improvement approach is proposed by integrating the SPT system with direct oxy-combusted (DOC) sCO_2 power cycle to enhance the overall efficiency and eliminate the need for the TES. In this paper, the off-design performance of two novel power cycle configurations that integrate SPT and DOC systems is investigated. The SPT system works as a preheater for the DOC system in the first configuration (S3) while works as a reheater in the second one (S4). The off-design analysis approach first verified and validated against published results and the results shows good agreement with error less than 1%. Also, the off-design analysis of these cycles is performed based on real ambient conditions and power demand profiles for two typical days in Qatar. The results show that the efficiency of S4 is considerably higher than S3, but S3 show better flexibility with the variation of the power demand profile. At 76% of the full load, the cycle efficiency is reduced by 5.64% in S4 and by 4.35% in S3. Moreover, at the design point conditions, the increase of the CIT reduces the cycle efficiency (by 8%) but also reduces the amount of the consumed fuel (by 15.8%). On the other hand, the increase of the TIT improves the cycle efficiency (by 8.6%) but also increases the consumed fuel by (57%).

1. Introduction

Among of the concentrated solar power (CSP) technologies (including parabolic trough collector, linear Fresnel reflector, parabolic dish system, and power tower), the solar power tower (SPT) has the potential to achieve high efficiency and large-scale power production due to its high achievable temperatures [1]. But, like the other CSP systems, the SPT systems require thermal energy storage (TES) to guarantee continuous operation and to provide a dispatchable power production according to the power demand. However, critical challenges still exist in the TES systems such as the high-temperature corrosion, expensive materials of TES components, requirement of auxiliary resources, temperature swing, and large size [2–6]. In addition, the TES forms an about 10% of the total cost of the CSP system which need significant reduction to be competitive with the fossil-fuel power technologies [7]. The ideal solution for these issues can be presented in three approaches (as shown in Fig. 1): (1) enhancing the overall efficiency of the power block, (2) enhancing the capacity of the TES with minimized capital and operational costs, and/or (3) eliminating the need for the TES system. The first approach is implemented by integrating the supercritical carbon dioxide (sCO_2) power cycle with the SPT (as discussed in section 1.1) [8]. The second approach is obtainable by developing alternative inexpensive materials with higher thermal capacity and stability (as discussed in section 1.2) [9,10]. The newly third approach is performed by integrating the SPT system with direct oxy-combusted (DOC) sCO_2 power cycle as proposed by Son et al. [7] and Xu et al. [11] (as discussed in section 1.3). More importantly, the last approach suffers from the lack for investigation at off-design conditions which is fundamental step to design efficient, reliable, flexible, and economic SPT-DOC system. Thus, this study concentrates on the off-design analysis of the third approach and compare it with conventional SPT-sCO_2 systems.

* Corresponding author.
E-mail address: wahib.alammari@qu.edu.qa (W.A. Al-Ammari).

https://doi.org/10.1016/j.renene.2021.08.047

Nomenclature

Symbols

A	heat transfer area, (m^2)
h	specific enthalpy, (kJ/kg)
$\dot{m}$	mass flow rate, (kg/s)
P	pressure, (MPa) (also Power (MW))
$\dot{Q}$	heat transfer rate, (kW)
T	temperature, (^oC & K)
U	overall heat transfer coefficient, (kW/m^2-^oC)
$\dot{W}$	power produced or consumed by a layout component, (kW)
η	energy, mechanical, or isentropic efficiency, (%)
ε	Emissivity of a surface, (Also effectiveness of HTR and LTR)

Subscripts

1, 2, 3	state points as shown in Fig. 2, and Fig. 3
CO_2	produced carbon dioxide at the outlet of the combustor
g	generator
hel	for the heliostat field
i	Inlet
max	maximum
min	minimum
net	net output
o	outlet
rCO_2	recycled carbon dioxide to the combustor
rec	for the solar receiver

Acronyms

ASU	air separation unit
CSP	concentrated solar power
DNI	direct normal irradiance
FC	fuel compressor
GC	gas compressor
GT	gas turbine
HPT	high pressure turbine
HTR	high temperature recuperator
LHV	lower heating value
LPT	low pressure turbine
LTR	low temperature recuperator
MC	main compressor
OC	oxygen compressor
PC	precooler
WS	water separator

1.1. Improving the overall efficiency of the SPT system

Despite the advantages of the SPT over the other CSP technologies, it is not economically competitive comparing to the fossil-fueled power plants [12–14]. One of the promised approaches to increase the efficiency and reduce the cost of the SPT system is to apply more efficient and compact power block [15,16]. Recently, the sCO_2 Brayton cycle is recommended as a substitute for the conventional steam Rankine cycle or the ideal gas Brayton cycle used in the SPT system due to the following features: the CO_2 is compressed near the critical point (7.38 MPa, 31 °C) which is considered as incompressible region thus less compression work is consumed; the high density of the sCO_2 in the entire power system leading to compact size for the cycle components; and the ability to works under dry cooling conditions which makes it easier to be applied in the SPT system located in droughty areas [17–20].

Different sCO_2 power cycle layouts have been proposed including the simple recuperated cycle, the dual recuperated cycle, the intercooling cycle, the partial cooling cycle, the precompression cycle and the recompression cycle [21–23]. The recompression cycle shows superior performance followed by the intercooled cycle [24]. However, the recompression cycle is not applicable if the sCO_2 cycle driven by an oxy combustion [25]. In this case, the intercooled layout is recommended. Several studies have been conducted to investigate the performance of the SPT system with these sCO_2 Brayton cycle in terms of energy, exergy, exergoeconomic, thermoeconomic, and optimization analyses [17,26–31]. Based on the results of the economic studies, the levelized cost of electricity (LCOE) of the SPT-sCO_2 power cycles equipped with TES (ranges between 14 and 26¢/kWh) still higher than that of the fossil-fueled power cycles [32–34]. Moreover, the initial capital investment of sCO_2 power cycles is higher than of stream Rankine cycles (by about 38%) [1]. Therefore, further improvements should be devoted to further reduce the capital investment of the SPT system.

1.2. Improving the performance of the TES system

The intermittency nature of solar energy, due to the weather as well as the seasonal variations, forms a major challenge in

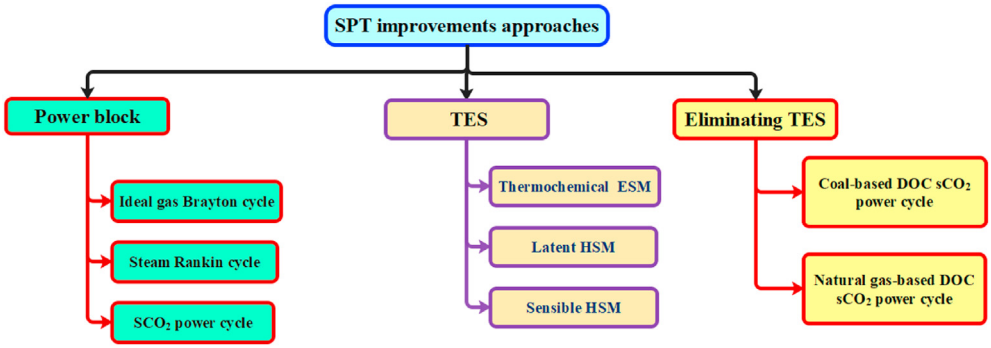

Fig. 1. Improvements approaches of the SPT system.

harvesting it for electricity generation. Also, the mismatch between solar energy availability and energy demand has negative effects on the overall efficiency of the system. To solve these issues, storing excess energy during peak sun hours to be used during nighttime for continuous electricity production in CSP plants. Therefore, a thermal energy storage (TES) system is added between the solar receiver and the primary heater of the power block. The TES system is capable of mitigating transient variations in the solar energy supply and shift the power production from peak solar irradiance hours to peak electricity consumption hours [35,36]. Achkari and Fadar [2] comprehensively reviewed the latest advances in the TES and CSP technologies. The have concluded that the latent heat and thermo-chemical heat storage systems still at a laboratory level and their development is still far from any proven design and material to be transferred to a commercial scale, especially for high temperature applications. In contrast, the liquid sensible heat storage (which mostly use molten salts) systems are the most widely used in CSP plants. However, most of the molten salts used in TES are highly corrosive which requires expensive corrosion-resistance containers [3]. At the same time, the cost of the CSP systems must be reduced to achieve competitive price of electricity compared to conventional power plants. Therefore, improving the optimal and thermal efficiencies of the CSP components, and developing alternative inexpensive materials for the TES are major factors to achieve comparable electricity price with other fossil-fueled plants.

1.3. Eliminating the need for TES in the SPT system

As mentioned before, Son et al. [7] have proposed a new approach to improve the performance of the SPT system and reduce the cost by integrating the SPT and the DOC, which in turns eliminates the need for a separated TES. In the integrated system, the SPT system works as a preheater to increase the temperature at the inlet of the oxy-combustor which further increases the temperature of the working fluid (sCO_2) to the desired temperature at the inlet of the turbine. In this way, the solar intermittency issue is solved without using TES. On the other hand, The DOC system uses the oxygen (which is generated by air separation unit (ASU)) instead of air to facilitate the separation of CO_2 from the flue gas and to avoid the production of thermal NO_x during the combustion which increase the concentration of CO_2 and makes it ready for storage. However, the stand-alone DOC system consumes a large amount of oxygen which brings substantial energy consumption (over 7% of the net output power of the cycle is consumed by the ASU) and high cost of operation. Therefore, the integrated SPT-DOC system also solves this issue by obtaining higher turbine inlet temperature but with significantly reduced fuel consumption (by 17–38% compared to the conventionally separated systems). However, Son et al. only performed preliminary calculation to estimate how much fuel consumption can be reduced due to the integration between the SPT and the DOC systems. Thus, a rigorous investigation for the integrated system at design and off-design condition still needed.

1.4. Off-design analysis of the sCO_2 power cycle integrated with SPT system

Many publications have been conducted within the aforementioned approaches. Although the design point performance of the SPT-sCO_2 system extensively studied, only few studies that investigate the off-design performance. In 2013, Dyreby et al. [37,38] have presented a flexible modeling methodology to estimate the performance of the sCO_2 power cycles under design and off-design ambient conditions (including the part-load operation). They have used semi-empirical models for the major cycle components including the compressor, turbine, and heat recuperators. They have concluded that high thermal efficiency can be obtained by the sCO_2 cycle over a range of off-design and part-load conditions. In 2018, Wright et al. [39] have presented the results of off-design performance modeling of sCO_2 power cycle driven by the waste heat of Titan 130 Gas Turbine. They have used the off-design simplified models described by Dyreby et al. [37,38] to complete the off-design modeling system. Furthermore, the have used four primary control mechanisms (to mitigate the effects of increases in ambient heat rejection temperature) including: varying the air-cooling fan speed, varying the boost compressor speed, varying the split-flow fraction, and controlling the compressor inlet pressure by using inventory control tanks or by using the filling tank reservoir. In 2019, Duniam and Veeraragavan [40] have investigated the off-design performance of 25MWe sCO_2 recompression power cycle with natural draft dry cooling tower for CSP generation. They reported that the system can maintain the design output power up to ambient temperature of 50 °C with 20% increase in the cycle mass flow rate and increasing turbine inlet temperature from 600 to 650 °C with 3.8% reduction in the efficiency. In 2020, Ty Neises [41] has presented a steady-state off-design modeling of a SPT-sCO_2 recompression power system with two-tank sensible-heat storage. He mentioned that optimizing the compressor shaft-speed improves the performance at cold ambient temperatures and part-load conditions. Also, in 2020, Yang et al. [42] have studied the off-deign performance of 50MWe simple sCO_2 power cycle integrated with SPT with molten-salt based TES system. They have applied the sliding pressure operation control strategy for the power cycle during the off-design operation. Recently, in 2021, Chen et al. [43] compares the design and off-design performances of six sCO_2 power layouts integrated with particle-based SPT system. Other off-design performance analyses have been applied on the sCO_2 power cycle integrated with other technologies including the parabolic trough collector [44], lead-cooled fast reactor [45,46], gas turbine [47], coal-fired boiler [48], solid oxide fuel cell, and molten carbonate fuel cell [49].

There are no available studies in open literature that investigate off-design performance of the integrated SPT and DOC systems which is the main objective of this work. It is important to visualize and compare the decrease of the system efficiency under off-design conditions with the standard SPT system. This is a major step before testing and applying control strategies that mitigate the efficiency decrease with the variation of the ambient conditions and power demand profiles. Also, the results of such analysis provide a guidance for the optimal design and operation of the power system. This paper investigates the off-design performance of a 50 MWe dry precooler-intercooled sCO_2 power cycle driven by integrated SPT and DOC systems in two different configurations. In the first configuration, the SPT works as a preheater to increase the temperature at the inlet of the combustor. In the second configuration, the SPT system works as a reheater to drive additional low-pressure turbine. The main aims and contributions of the present study include:

- Applying the off-design analysis of the proposed configurations and comparing it with similar analysis for a simple recuperative sCO_2 power cycle driven by SPT equipped with molten-salt-based TES.
- Simulating the off-design performance of the proposed configurations under harshly climate conditions and power demand variations in Qatar (by using scaled data for the maximum power demand day (7 Sept.) and minimum power demand day (1 Feb.) in 2016).

- Investigating the feasibility of reducing the solar field size to make it useful around the year with DOC forms the backbone of the energy source.
- Investigating the performance of the cycle configurations under different compressor and turbine inlet temperatures.
- Investigating the effect of the ambient temperature change on the performance of both SPT system and power block of these configurations.

The rest of the manuscript is organized in 4 more sections. Section 2 describes the proposed configurations detailing their technical characteristics and advantages. Section 3 presents the design and off-design mathematical models of the proposed configurations. Also, verification and validation of the developed models are presented in section 3. In section 4, the off-design analyses are carried out and compared with similar SPT system. The main findings and conclusions are summarized in section 5.

2. Description of the integrated SPT − DOC sCO_2 power cycle configurations

The authors of the present study have investigated the design performance of five configurations (S1 to S5) (See Fig. A1 in the Appendix). The power block of these cycles is mainly composed of an intercooled dual recuperative sCO_2 power cycle. The major difference between these cycles is in the energy source that drives each of them. S1 is driven by stand-alone DOC, S2 is driven by stand-alone SPT system, while the new proposed configurations (S3, S4, and S5) are driven by an integrated SPT-DOC system. Therefore, the first two configurations (S1 and S2) are considered as basic systems for comparison and validation purposes. In S3 (shown in Fig. 2), the SPT system works as a preheater to raise the temperature of the recycled sCO_2 from the temperature at state 11 to higher temperature at state 11'. In this way, less amount of fuel and oxygen will be needed to obtain the desired temperature at the inlet of the turbine (state 1). While in configuration S4 (shown in Fig. 3), the SPT system works as a reheater (process 2-1′) to drive a low-pressure turbine (LPT) (1' -2'), while the DOC system drives the HPT (1–2). In S4, it should be noted that the solar receiver works at an intermediate pressure, and the CO_2 stream flow through it involves water vapor. In S5, the recycled sCO_2 flow is split at state 11 into two streams, one of them is heated by the DOC and the other stream is heated by the SPT system. Thorough energetic, exergetic, exergoeconomic, thermoeconomic and optimization analyses was conducted for these configurations (S1 to S5) at design conditions. The optimization process was performed by single- and multi-optimization analyses to identify the best operating conditions for these configurations. The optimization methodology is presented in the Appendix (Fig. A2). The multi-objective optimization results revealed that S4 has thermal efficiency of 55.29% at LCOE of

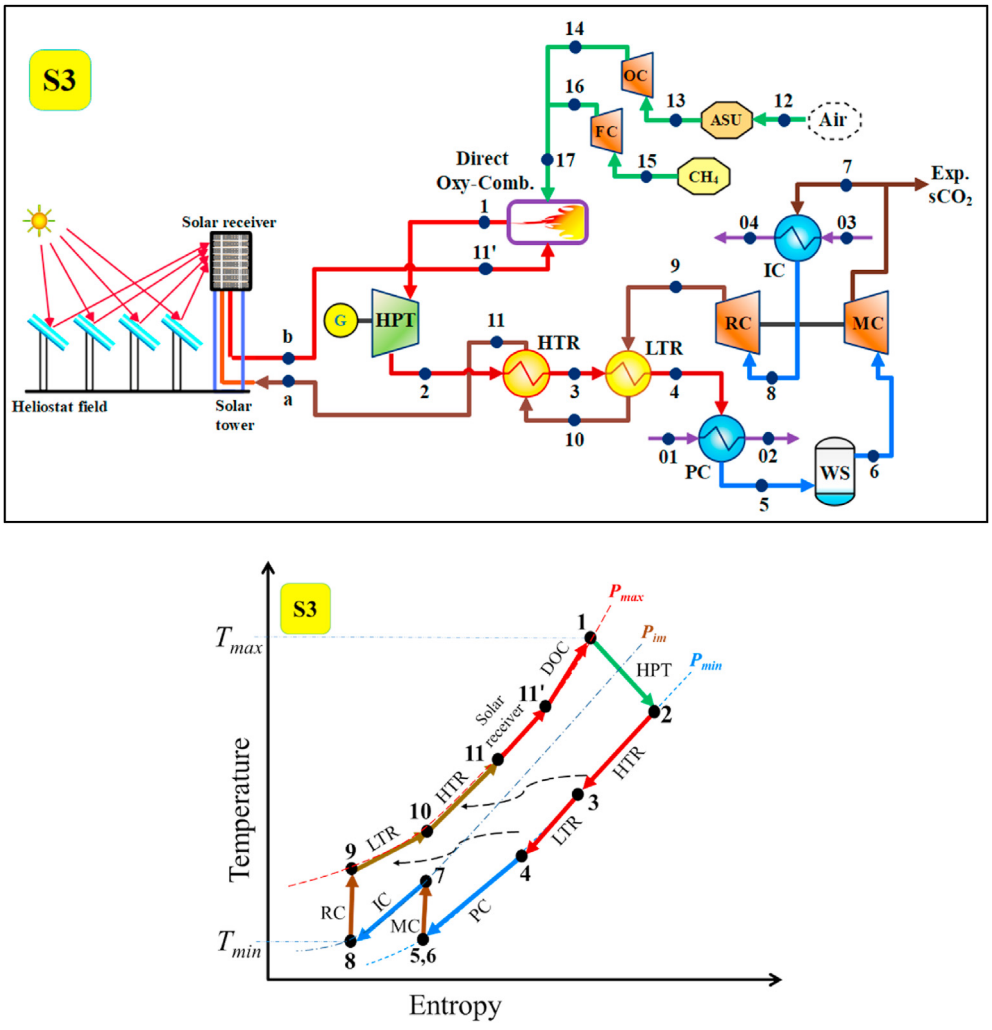

Fig. 2. Hybrid SPT and DOC sCO_2 power system configuration and T-S diagram where the SPT system works as a preheater (S3).

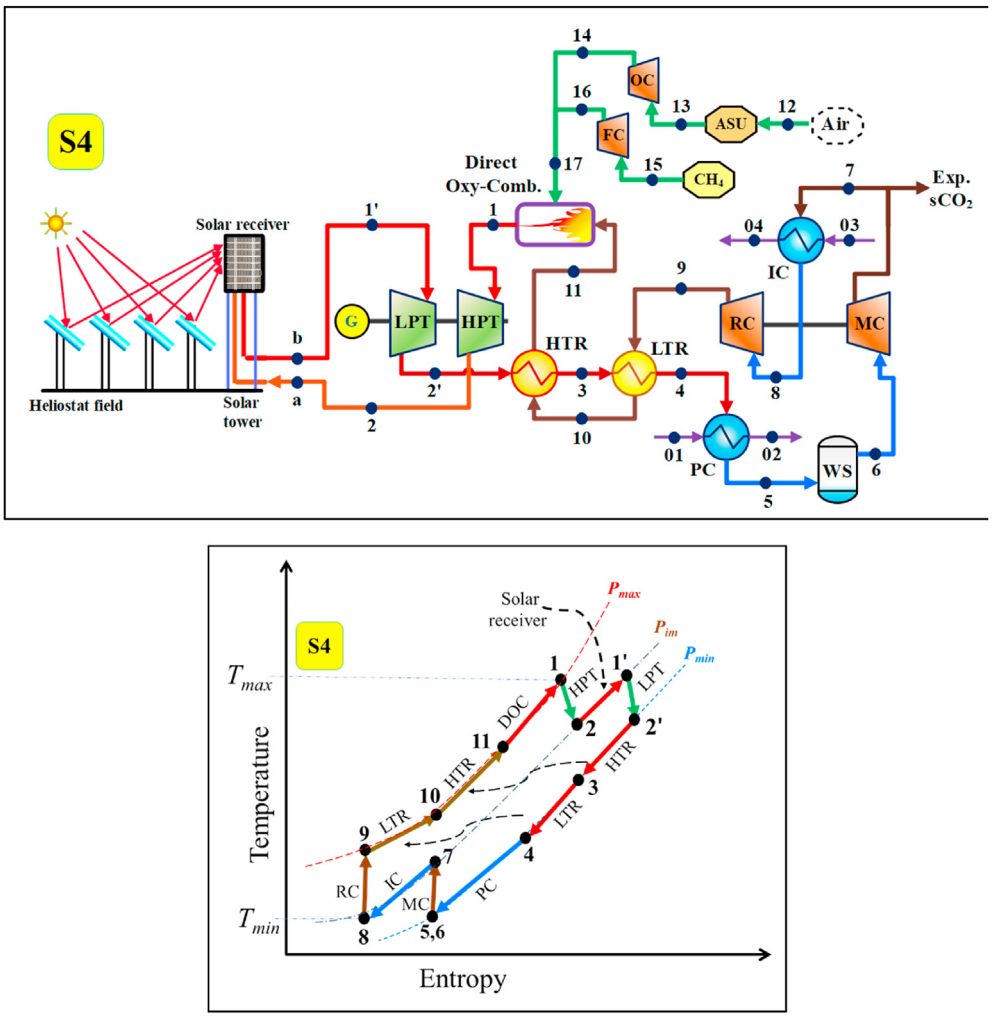

Fig. 3. Hybrid SPT and DOC sCO_2 power system configuration and T-S diagram where the SPT system works as a reheater (S4).

7.705¢/kWh compared to 40.54% at 6.351¢/kWh for S1; 45.56% at 7.864¢/kWh for S2, 52.90% at 7.970¢/kWh for S3, and 48.72% at 8.138¢/kWh for S5. As S3 (Fig. 2) and S4 (Fig. 3) show superior performance over the other configurations (S1, S2 and S5), they are selected for further analysis at off-design and part-load operation conditions in this study.

Both of S3 and S4 are able to solve the intermittency issue of the SPT by controlling the flow rate of the natural gas at the full-load or part-load operation even with the variation of the ambient conditions. Therefore, with the presence of the DOC system, the SPT system no longer needs thermal storage system for backup power. Also, at part-load operation, the sliding pressure operation control strategy (which is common and mature strategy for modern power plants) is applied to meet the varying power demand. Moreover, the integrated systems (S3 and S4) have met the emission requirements (zero CO_2 emissions) under improved cycle performance.

In both configurations (S3 and S4), the turbine outlet flow passes through the high temperature recuperator (HTR) (process 2–3) and the low temperature recuperator (LTR) (3–4) to heat the recycled sCO_2 (processes 9–10, and 10–11) before entering the DOC (state 11). At state 4, the low-pressure flow passes through the precooler (PC) (4–5) and the water separator (5–6) to remove the water content from the sCO_2 stream. Then, the sCO_2 is compressed by the main compressor (MC) to an intermediate pressure (higher than 75 bar) which is suitable for exporting the excess CO_2 resulted from the combustion process at state 7. Then, the CO_2 flow is cooled by an intercooler (IC) (7–8) and recompressed by a recompressor (RC) to a maximum cycle pressure (200 bar–300 bar) (process 8–9). The high-pressure sCO_2 flow is then directed to the recuperators (9–11) and enters the DOC to control the temperature of the oxy-combustion products at state 1. With the presence of the recycled sCO_2, a pressurized fuel (16) is mixed with compressed oxygen (17), which is generated by an air separation unit (ASU) (process 12–13) and combusted in the oxy-combustor. The exhaust flow is directed to the inlet of the turbine (1) to expand to the lower cycle pressure in the HPT of S3 or to an intermediate pressure in S4 then directed to the SPT to reheat the exhaust flow and expand it to the low cycle pressure through the LPT.

3. Mathematical model

To investigate the performance of S3 and S4 under off-design conditions, the design models of both configurations are adapted here from the previous work. Then the off-design models of the turbomachinery and heat exchanger components are integrated with these models and validated against available data in the literature with real measured climate conditions and power demand variation. The developed models are based on the following assumptions.

- Pure methane and oxygen were assumed for the oxy-combustion process.
- Variations of the kinetic and potential energies are negligible.
- Heat losses from the cycle components (except the solar field components) to ambient air are negligible.
- To gather more reflected light from the edge of the solar field, a 360° external cylinder receiver is applied.

3.1. Heliostat field and receiver

Referring to Figs. 2 and 3, the total incident solar heat on the heliostats field ($Q_{in,sol}$) is given as [42]:

$$Q_{in,sol} = DNI \cdot A_{hel} \tag{1}$$

where DNI and A_{hel} are the direct normal irradiance and the total area of the heliostat field, respectively. The heat delivered from the heliostats and absorbed by the receiver ($Q_{in,rec}$) is calculated as [42]:

$$Q_{in,rec} = Q_{in,sol} \cdot \eta_{hel} \cdot \alpha_{rec} \tag{2}$$

where η_{hel}, and $\cdot\alpha_{rec}$ are the energetic efficiency of the heliostat field and the absorptivity of the receiver. Part of the heat absorbed by the receiver is delivered to the working fluid of the cycle (Q_{rec,sCO_2}) and the other part is lost to the ambient by convection ($Q_{conv,rec}$) and radiation ($Q_{rad,rec}$). The overall energy balance of the receiver is expressed as follows [42]:

$$Q_{in,rec} = Q_{rad,rec} + Q_{conv,rec} + Q_{rec,sCO_2} \tag{3}$$

The heat loss due to radiation ($Q_{rad,rec}$) is calculated as [42]:

$$Q_{rad,rec} = \sigma \cdot \varepsilon_{rec} \cdot A_{rec}\left((T_{rec}+273)^4 - \left(T_{sky}+273\right)^4\right) \tag{4}$$

where σ is the Stefan-Boltzmann constant (5.67×10^{-8} W/m^2-K^4), ε_{rec} is the receiver emissivity, A_{rec} is the surface area of the receiver, T_{rec} is the temperature of the external surface of the receiver, and T_{sky} is the effective temperature of the sky. T_{sky} can be expressed in terms of the ambient air temperature (T_{am}) as follows [50]:

$$T_{sky} = 0.0552 \times (T_{am})^{1.5} \tag{5}$$

The heat loss due to natural and forced convection ($Q_{conv,rec}$) with the ambient air is calculated as [42]:

$$Q_{conv,rec} = h_{conv,rec} \cdot A_{rec}(T_{rec} - T_{am}) \tag{6}$$

where $h_{conv,rec}$ is the convection heat transfer coefficient, which can be expressed in terms of the wind speed (V_{wind}) as [51]:

$$h_{conv,rec} = 2.8 + 3 \cdot V_{wind} \tag{7}$$

Considering the thermal resistances between the outer surface of the receiver and the sCO_2 passing across the receiver, the heat transmitted to the sCO_2 from the receiver surface (Q_{rec,sCO_2}) is calculated as:

$$Q_{rec,sCO_2} = \frac{T_{rec} - \overline{T}_{rec,sCO_2}}{R_{cond,rec} + R_{conv,sCO_2}} \tag{8}$$

where $\overline{T}_{rec,sCO_2}$ is the average temperature of the sCO_2 across the receiver which is expressed as $\overline{T}_{rec,sCO_2} = \frac{T_a + T_b}{2}$; $R_{cond,rec}$, and R_{conv,sCO_2} are the conductive resistance of the receiver tubes and the convective resistance of the sCO_2, respectively. Also, Q_{rec,sCO_2} can be expressed in terms of the mass flow rate and the specific heat of the sCO_2 (to keep the model in terms of terminal temperatures which facilitate the iterative solution process) as:

$$Q_{rec,sCO_2} = \dot{m}_a \cdot \bar{c}_{p,ab}(T_b - T_a) \tag{9}$$

3.2. Design model of the sCO_2 power cycle

The energy models of the sCO_2 power cycle components were developed by applying the mass and energy conservation principles on the control volume of each component such that [52]:

$$\sum \dot{m}_i = \sum \dot{m}_o \tag{10}$$

$$\sum \dot{Q} + \sum \dot{m}_i h_i = \sum \dot{W} + \sum \dot{m}_o h_o \tag{11}$$

Table 1 summarizes the mass and energy balance equations of each component of the studied sCO_2 power cycle configurations. It should be mentioned that the mass flow rate of the oxygen required for the oxy-combustion process and the mass flow rate of the CO_2 at the exit of the combustor were calculated based on the real combustion reaction as explained by Sleiti et al. in Refs. [24,25]. To take into account the dramatic change of the specific heat of the CO_2 with temperature variation, the calculations of the HTR and LTR were obtained based on discretized effectiveness-based model as explained in detail by Sleiti et al. in Refs. [24,25].

The thermal efficiency of each configuration is given in terms of the net output power ($\dot{W}_{net}$) and the total input power ($\dot{Q}_{in}$) for each configuration as:

$$\eta_{s-CO_2} = \frac{\mathrm{P_{net}}}{\dot{Q}_{in}} \tag{14}$$

where the equations of $\dot{W}_{net}$, and $\dot{Q}_{in}$ are given in Table 1.

3.3. Off-design model of the sCO_2 power cycle

The off-design models developed by Dyreby et al. [37] for the turbomachinery and recuperator components of sCO_2 power cycle were adapted here for the off-design analyses of the proposed cycles. This off-design model was developed based on experimental data being developed for use in a sCO_2 power cycle at the Sandia National Laboratory [37]. In this model, the modified flow coefficient (φ^*), ideal head coefficient (ψ^*), and efficiency (η^*) are given as shown in equations (15)–(17), respectively.

$$\varphi^* = \frac{\dot{m}_{CO2}}{\rho U_c D_c^2}\left(\frac{N}{N_{design}}\right)^{1/5} \tag{15}$$

$$\psi^* = \frac{\Delta h_i}{U_c^2}\left(\frac{N_{design}}{N}\right)^{(20\varphi^*)^3} \tag{16}$$

$$\eta^* = \eta\left(\frac{N_{design}}{N}\right)^{(20\varphi^*)^5} \tag{17}$$

where $\dot{m}$, and ρ are the mass flow rate and density of the fluid at the inlet of the compressor, respectively. U_c, D_c, N, and N_{design} are the tip speed of the rotor, diameter of the rotor, shaft speed, and the design shaft speed, respectively. Δh_i is the ideal enthalpy rise across the compressor. The mass flow rate across the turbine is given as:

Table 1
Energy balance equations of the main components of the proposed scenarios.

Component/process	Mass and energy balance equation
Direct Oxy-Comb.	$\dot{Q}_{oc} = \dot{m}_1 h_1 - \dot{m}_{11} h_{11} - \dot{m}_{16} h_{16} - \dot{m}_{14} h_{14}$; $\dot{m}_1 = \dot{m}_{11} + \dot{m}_{16} + \dot{m}_{14}$ $\dot{m}_1 = \dot{m}_{CO_2} + \dot{m}_{wv}$; $\dot{m}_{11} = \dot{m}_{rCO_2}$; $\dot{m}_{16} = \dot{m}_f$; $\dot{m}_{14} = \dot{m}_{O_2}$ $\dot{m}_{O_2} = 4 \cdot \dot{m}_f$ $\dot{m}_{CO_2} = \dot{m}_{rCO_2} + 2.75 \cdot \dot{m}_f$ $\dot{Q}_{oc} = \dot{m}_f \cdot LHV_f$
HPT	$\dot{W}_{HPT} = \eta_{t,HPT} \times \dot{m}_1 (h_1 - h_{2s})$, $\eta_{t,HPT} = \dfrac{(h_1 - h_2)}{(h_1 - h_{2s})}$
LPT	$\dot{W}_{LPT} = \eta_{t,LPT} \times \dot{m}_1 (h_{1'} - h_{2's})$; $\eta_{t,LPT} = \dfrac{(h_{1'} - h_2)}{(h_{1'} - h_{2s})}$
MC	$\dot{W}_{MC} = \dot{m}_6 (h_{7s} - h_6)/\eta_{MC}$; $\dot{m}_6 = \dot{m}_1 - \dot{m}_{wv}$; $\eta_{MC} = \dfrac{(h_7 - h_{6s})}{(h_7 - h_6)}$
RC	$\dot{W}_{RC} = \dot{m}_8 (h_{9s} - h_8)/\eta_c$; $\dot{m}_8 = \dot{m}_7 - \dot{m}_{exp,CO_2}$; $\eta_{RC} = \dfrac{(h_9 - h_{8s})}{(h_9 - h_{8s})}$
OC	$\dot{W}_{OC} = \dot{m}_{14} (h_{14s} - h_{13})/\eta_c$
FC	$\dot{W}_{FC} = \dot{m}_{16} (h_{16s} - h_{15})/\eta_c$
HTR	$\dot{Q}_{HTR} = \dot{m}_1 (h_2 - h_3)$
	$\dot{Q}_{HTR} = \dot{m}_{11} (h_{11} - h_{10})$
LTR	$\dot{Q}_{LTR} = \dot{m}_8 (h_{10} - h_9)$
	$\dot{Q}_{LTR} = \dot{m}_3 (h_3 - h_4)$
PC	$\dot{Q}_{PC} = \dot{m}_1 (h_4 - h_5)$
	$\dot{Q}_{PC} = \dot{m}_{01} (h_{02} - h_{01})$
IC	$\dot{Q}_{IC} = \dot{m}_7 (h_7 - h_8)$
	$\dot{Q}_{IC} = \dot{m}_{03} (h_{04} - h_{03})$
ASU	$\dot{W}_{ASU} = \dot{m}_{O_2} \times SPC_{ASU}$
Net output power	For S3: $P_{net} = \dot{W}_{HPT} - \dot{W}_{MC} - \dot{W}_{RC} - \dot{W}_{OC} - \dot{W}_{FC} - \dot{W}_{ASU}$; For S4: $P_{net} = \dot{W}_{HPT} + \dot{W}_{LPT} - \dot{W}_{MC} - \dot{W}_{RC} - \dot{W}_{OC} - \dot{W}_{FC} - \dot{W}_{ASU}$;
Total input power	$\dot{Q}_{in} = \dot{Q}_{oc} + \dot{Q}_{in,rec}$

$$\dot{m}_{CO2} = C_s A_{nozzle} \rho_{out} \tag{18}$$

where C_s is the spouting velocity (the velocity that could be achieved if the fluid isentropically expanded to the lower pressure through an ideal nozzle). A_{nozzle} is the effective nozzle area, and ρ_{in} is the fluid density at the turbine outlet. To obtain the isentropic at the off-design conditions ($\eta_{t,off}$), first, the ideal aerodynamic efficiency is calculated by Eq. (19) as follows:

$$\eta_{aero,ideal} = 2\nu\sqrt{1-\nu^2} \tag{19}$$

where ν is defined as the ratio of tip velocity to the spouting velocity of the turbine as follows:

$$\nu = \frac{U_t}{C_s} \tag{20}$$

$$C_s = \sqrt{2\Delta h_i} \tag{21}$$

Then, $\eta_{aero,ideal}$ is substituted into Eq. (20) to obtain $\eta_{t,off}$ as follows.

$$\eta_{t,off} = \eta_{design} \eta_{aero,ideal} \tag{22}$$

Given that the mass flow rate of sCO_2 changes under the off-design condition, the off-design performance can be hold by the relationship between the off-designed (UA) and designed (UA) of the recuperators which is given as:

$$\frac{UA_{off}}{UA_{design}} = \left(\frac{\dot{m}_{CO2,off}}{\dot{m}_{CO2,design}} \right)^{0.8} \tag{23}$$

3.4. Solution procedures

When the model of the intercooled oxy-combusted sCO_2 power cycle is integrated with solar field model, three variables will be interacted between the two models which are the mass flow rate of the sCO_2, the temperature of the fluid at the inlet (T_a) and outlet (T_b) of the receiver. Therefore, after the input parameters are defined (as presented in Table 2), the solution procedures shown in Fig. 4 are performed simultaneously. The solution start by inserting all of the input parameters for the solar field and the power block. Then, two parameters logically assumed which are the temperature of the receiver (outer surface) and the maximum pressure at the inlet of the turbine. Then the calculations code is run (which is built by using Engineering Equation Solver (EES) in this study) until the receiver load calculated from Eq. (3) converge with that calculated by Eq. (3) and the calculated output power converge with the input power demand with error less than 0.1%. Once the error brought below 0.1%, the results saved and transferred to Excel for further analysis.

3.5. Verification and validation

To validate the procedures and results of the off-design analysis of the present study, we have verified the off-design results of a 50MWe simple recuperated sCO_2 power cycle (SRC) integrated with molten-salt based SPT system published by Yang et al. [42]. They have reported the off-design ambient conditions (direct normal irradiance (DNI) and ambient temperature (T_{am})) for summer solstice (SS) and winter solstice (WS) for a typical remote and drought city in China (Delingha, 37.4° N, 97.4° E) as shown in Fig. 5 (a) and the power demand data for these days as shown in Fig. 5 (c). The results of the receiver efficiency and cycle efficiency for both SS and WS obtained by our model are compared with those reported by Yang et al. [42] as shown in Fig. 5 (b) and Fig. 5 (c), respectively. The

Table 2
Design point parameters.

	Parameter	Range/Design value
Solar field parameters	Direct Normal Irradiance, *DNI* (W/m^2)	550
	Heliostat field efficiency, η_{hel} (%)	62
	Heliostat height, H_{hel} (m)	12
	Receiver diameter, D_{rec} (m)	15
	Receiver height, H_{rec} (m)	19.5
	Receiver absorptivity, α_{rec}	0.94
	Receiver emissivity, ε_{rec}	0.85
	Tower height, H_{tow} (m)	220
	Ambient air temperature, T_a (°C)	45
sCO_2 power cycle parameters	Net output power, $\dot{W}_{net}$ (MW)	50
	Maximum cycle pressure, P_{max} (MPa)	20-30/25
	Minimum cycle pressure, P_{min} (MPa)	7.5
	Minimum cycle temperature, T_{min}	40-65/45
	Turbine isentropic efficiency, η_t [53]	93
	Compressor isentropic efficiency, η_c (%) [53]	89
	LHV_f, (kJ/kg)	50500
	Pressure drops across the DOC, (%) [54]	3
	Pressure drops across the HTR and LTR (hot side), (%) [54]	3
	Pressure drops across the HTR and LTR (cold side), (%) [55]	1
	Pressure drops across the PC and IC, (%) [55]	2
	Specific power consumption of the ASU, SPC_{ASU}, (kW/(kg$O_{2/s}$)) [56]	900
	Compressor diameter, D_c (m)	0.48
	Compressor shaft speed, $N_{c,design}$, (rpm)	13000
	Turbine diameter, D_t, (m)	0.60
	Turbine shaft speed, $N_{t,design}$, (rpm)	13000
	Design recuperator effectiveness, ε_r, (%) [57]	95

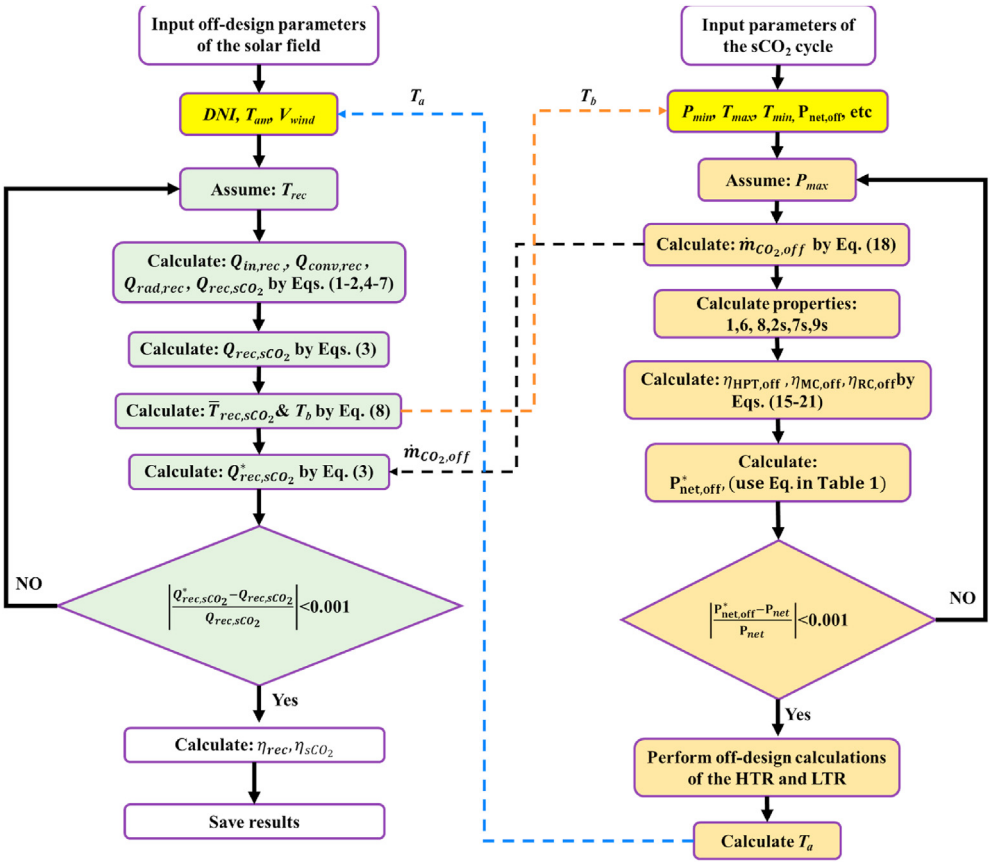

Fig. 4. Flow chart of off-design solution procedures.

results of the present study show good agreement with the reference data with difference less than 1% which may be attributed to the differences in the solar field model such as the equations used to calculate the heat transfer coefficient with the ambient air (Eq. (7)) which is considered more conservative than that used by Yang et al. [42].

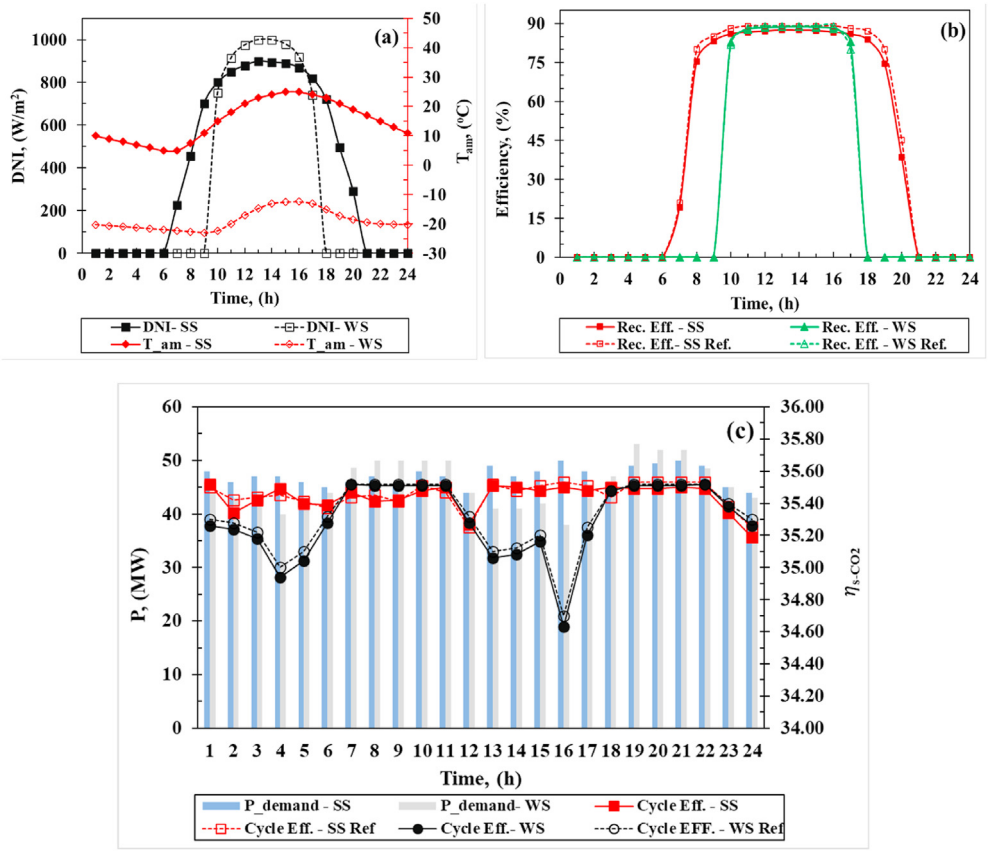

Fig. 5. (a) Off-design ambient conditions provided by Yang et al. [42], (b) verification of the receiver efficiency calculations in SS and WS, and (c) verification of the cycle efficiency with the variation of the power demand in SS and WS.

Furthermore, the model of the power block is modified to match the configurations of a simple recuperative and recompression sCO_2 power cycles to analyze their off-design performance using the same control strategy applied by Dyreby et al. [37] (by adjusting the compressor inlet pressure, main shaft speed, and the recompression fraction). The obtained results are compared with those published by Dyreby et al. [37] and show good agreement as shown in the Appendix (Fig. A3).

4. Results and discussion

In this section, the off-design performance of S3 and S4 are compared to the performance of the SRC studied by Yang et al. [42] under the same conditions of Delingha city (section 4.1). Then, the off-design performance of the solar field in S3 and S4 is investigated and compared to the performance of the SRC based on ambient conditions and power demand variations for typical days in Qatar (section 4.2). Also, the off-design performances of the power blocks (S3 and S4) under different compressor inlet temperatures (CIT) and turbine inlet temperatures (TIT) are presented in section 4.3. Finally, the effect of the ambient temperature on the operating parameters of the solar receiver is discussed in section 4.4.

4.1. Comparison

Fig. 6 compares the performance of S3 and S4 relative to the performance of the SRC investigated by Yang et al. [42] (abbreviated as Ref. in the legend of Figs. 4 and 5) with the variation of the net output power (P_{net}). Fig. 6 (a) shows that the cycle efficiency of S3 and S4 is higher than of the Ref. cycle by 7.63% and 14.91% (based on average values), respectively. The superior performance of S3 and S4 compared to Ref. cycle attributed to utilization of the intercooling configuration which significantly reduces the compression power and improves the cycle efficiency. Although the Ref. cycle is simpler in terms of turbomachinery components, S3 and S4 simplify the integration with the SPT system using direct connection with the DOC system without TES. In this way, at full load demand, the variation of the solar field can be manipulated by controlling fuel flow rate of the combustor. If the cycle operates under part-load conditions with excess solar energy, the flow rate of the fuel turn off and the pressure sliding control strategy is applied to match the demand power. If the cycle works under part-load conditions with the absence of the solar energy, the recycled sCO_2 flow can be bypassed directly to the DOC system and the same strategy is followed to match the demand power.

As the intercooling process minimizes the compression power by maintaining dense behavior of the sCO_2 across the compressor, it also reduces the required amount of the working fluid (sCO_2) compared to the conventional SPT-sCO_2 power systems as shown in Fig. 6 (b). Consequently, the temperatures of the recycled sCO_2 at the outlet of HTR in S3 and S4 are higher than in Ref. as shown in Fig. 6 (c). This in turns has a negative effect on the performance of the solar field in S3 and S4 by minimizing the useful energy received from the receiver. However, the reduction of the compression power has dominated the overall thermal efficiency of S3 and S4 and enhanced it significantly compared to Ref. cycle. Minimizing the mass flow rate of the sCO_2 in S3 and S4 keeps the temperatures across the cycle components at higher level than in

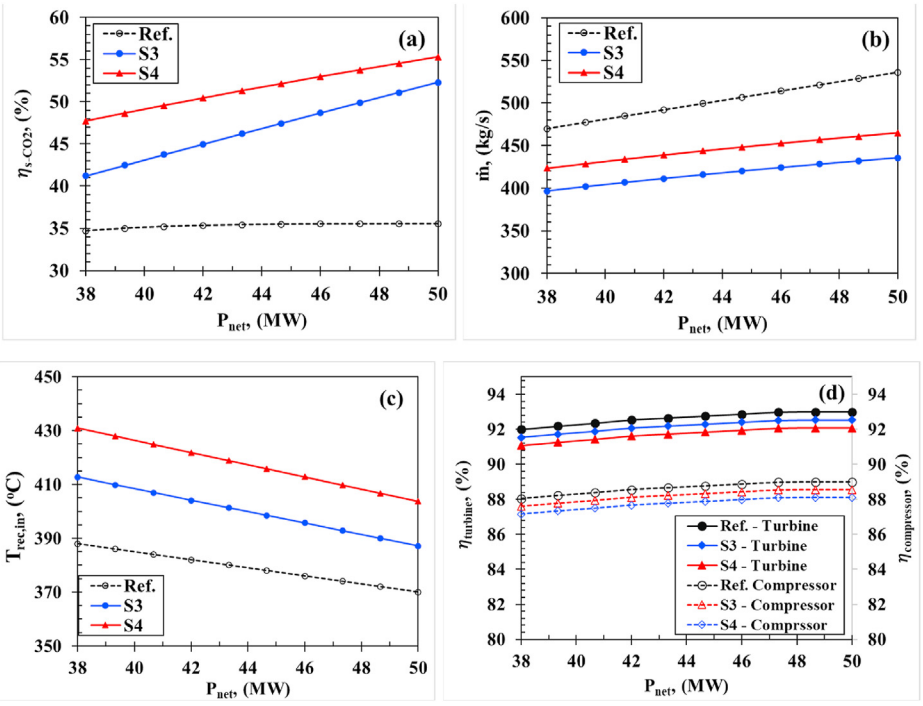

Fig. 6. The performance of S3 and S4 compared to the SRC investigated by Yang et al. [42] in terms of the (a) cycle efficiency, (b) fluid temperature at the inlet of the receiver, (c) mass flow rate of sCO_2, and (d) the off-design isentropic efficiencies of the turbomachinery components (turbines and compressors).

Ref. cycle which has a slightly reduces the off-design isentropic efficiency of the turbomachinery components as shown in Fig. 6 (d). This conclusion is confirmed by that the isentropic efficiencies of S3 is higher than of S4 as the temperatures across S4 components are higher than of S3 (see Fig. 6 (d) as example).

4.2. Off-design analysis of the solar field

To investigate the off-design performance, real ambient conditions and variable power demand data are needed. Therefore, available data for the ambient conditions and power demand variation of two typical days in Qatar (namely, 7 Sept. and 1 Feb.) were used for the analysis [58,59]. These days were selected since the maximum power demand along the year (2016) is noted in (7 Sept.) and minimum power demand in (1 Feb.). Fig. 7 (a) shows the daily variation of DNI and T_{am} in these two days. Also, the power demand profiles of them were scaled from the original profiles to be fit with a 50 MW power cycle and presented in Fig. 7 (c) (bar columns). The legend code for the curves in Fig. 7 is as follows: solid lines for 7 Sept. and dashed lines for 1 Feb.; red-square lines for S3 and black-rectangle lines for S4; green and blue lines for the solar field input data. Based on these data, the off-design performance of the solar field (in terms of the receiver efficiency) and the power cycle (in terms of the overall cycle efficiency $\eta_{s\text{-}CO2}$) are presented in Fig. 7 (b) and Fig. 7 (c), respectively. As shown in Fig. 7 (b), the receiver efficiency in S3 is higher than in S4 by about 10.23% at the peak of the DNI. This is attributed to the higher temperature of the recycled sCO_2 at the inlet of the receiver (as shown in Fig. 6 (c)) which minimizes the received energy from the receiver and thus reduces its thermal efficiency. Furthermore, it can be noted that the receiver efficiency in both 7 Sept. and 1Feb. slightly different from each other since the effect of the ambient temperature reduction in 1 Feb. is compensated by the increase of the DNI in the same day which levelized the receiver efficiency at 78% in S3 and 67 in S4 for 8 h (from 8:00 to 16:00).

It is a straightforward that the power demand variation affects the cycle efficiency with higher efficiency occurs at higher power demand and the opposite is true (see Fig. 7 (c)). However, the turbine inlet pressure can be controlled (following the sliding control pressure strategy) such that the cycle efficiency maintained at higher values than the conventional SPT-sCO_2 power systems. For instance, in S4- 7 Sept., the cycle efficiency is varying from a maximum value (55.68% at 50 MW, 14:00) to a minimum value (50.04% at 50 MW, 14:00). This implies that as S4 operates at 76% of the full load, its efficiency is reduced by 5.64% comparing to the full load efficiency. This difference is reduced to 4.35% in S3-7 Sept. which means that S3 is more flexible than S4 with the power demand variation. Further reduction of the power demand to about 38.3%–50% of the full load (in 1 Feb.) reduced the cycle efficiency by about 7.08% in S4 and 6.51% in S3 compared to the efficiencies at higher power demand (7 Sept.). Although the cycle efficiency of the proposed configurations with the power demand variation still higher than of the conventional SPT systems, the control strategy needs more improvements to mitigate the decrease of the cycle efficiency as the demand moves far from the full-design capacity. Therefore, further investigation for the proposed configurations with different and advanced control strategy is recommended.

Fig. 8. (a) compares the power demand of Delingha city (China) reported by Yang et al. [42] and Qatar in summer and winter solstices. In summer solstice, the power demand of Delingha and Qatar slightly differ from each other. In winter solstice, the power demand of Qatar is 44.5% less than of Delingha city. Accordingly, the cycle efficiency of the SRC with TES in winter solstice of Qatar is less than in winter solstice of Delingha by about 1.54% as shown in Fig. 8. (b). The large difference between the power demand in winter and summer (in Qatar) significantly reduce the efficiency of the cycle and add more complexity to the design of the TES and cycle components. The large demand in summer dictate large solar field and TES capacity which have no benefits in winter with sharp low demand in winter. To overcome this challenge, the solar field

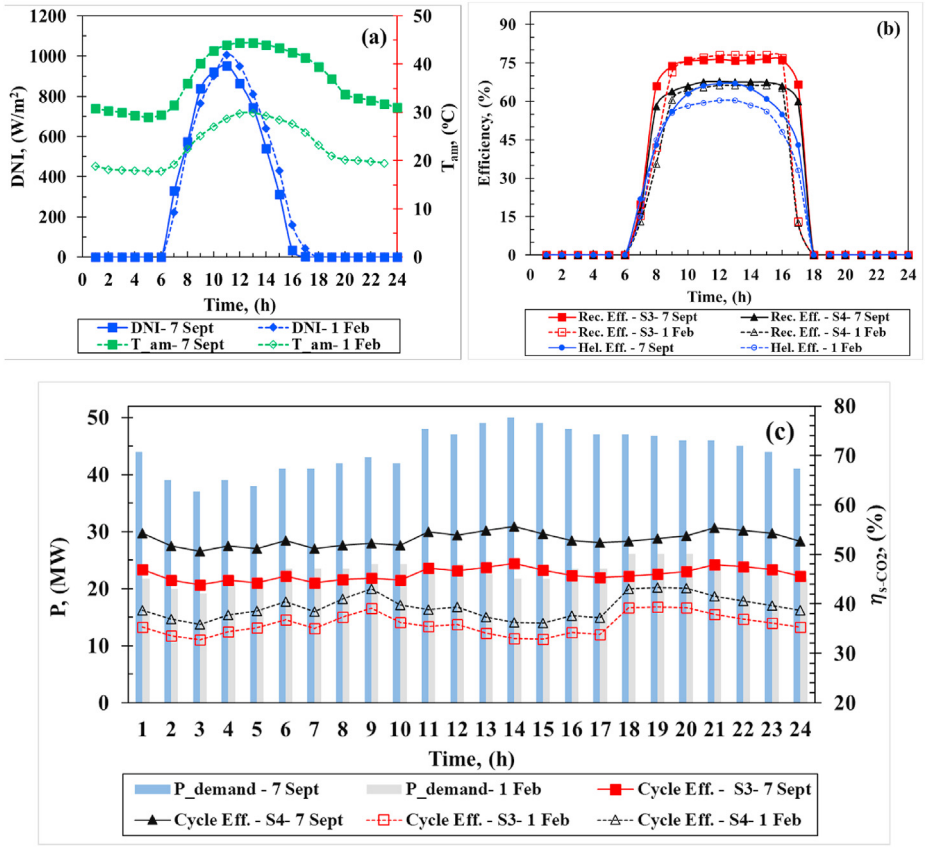

Fig. 7. (a) Ambient conditions, (b) solar field performance, and (c) cycle efficiency with the variation of the power demand for two typical days in Qatar: 7 Sept (maximum power demand day) and 1 Feb (minimum power demand day) in 2016.

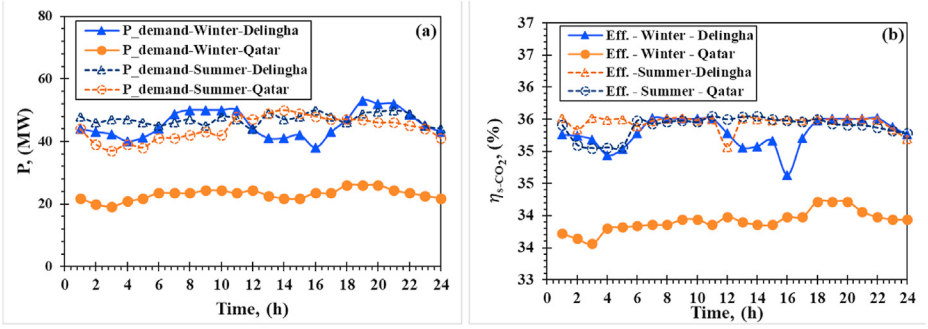

Fig. 8. Comparison between (a) power demand of Delingha city and Qatar and (b) corresponding efficiency of the SRC equipped with TES.

can be designed based on the power demand of winter solstice and the additional power required in summer solstice is provided by the direct oxy-combustor DOC proposed in S3 and S4 as shown in Fig. 9.

Fig. 9 ((a) and (b)) shows the performance of S3 and S4 in summer and winter solstices of Qatar and compares it to the performance of the SRC with TES under the same conditions. It is found that the thermal efficiency of S3 and S4 (with DOC) are higher than of the SRC (with TES) by 8.81% as a minimum and 22.11% as maximum. Although the thermal efficiency of S3 and S4 considerably change with the variation of the power demand during the day, both configurations still have more efficient performance than the SRC in both summer and winter solstices.

In the SRC with TES, the solar field is designed based on the maximum power demand (50 MW, summer) which dictate very large size than required at the minimum power demand (25 MW, winter). In contrast, incorporating the DOC with the SPT system make it possible to design the solar field based on the minimum power demand such that the solar field being useful all the year at all conditions. Meanwhile, the extra power required at summer conditions easily provided by the DOC which is more reliable than the TES. Table 3 shows the performance of S3 and S4 at different power demand and solar field sizes compared to the basic size of the SRC with TES. From Table 3, it can be noted that S3 and S4 show higher efficiency at N_{hel} of 2473 compared to N_{hel} of 4946 in both power demand cases (50 MW and 25 MW). At the same time, the fuel consumption is increased to about two times higher than at N_{hel} of 4946. However, the cycle efficiency is more efficient at

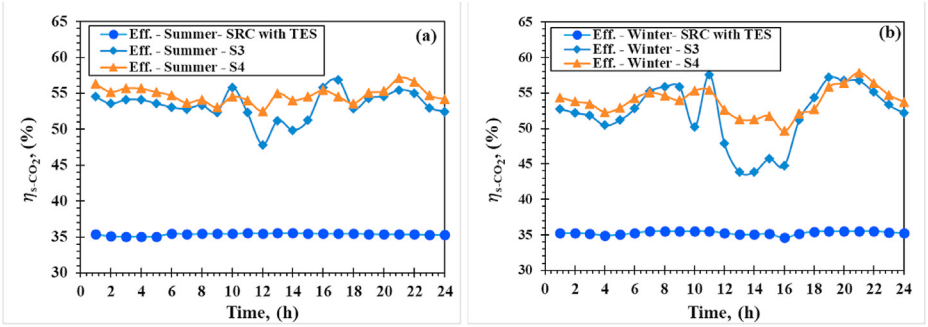

Fig. 9. Cycle efficiency of the SRC with TES, S3, and S4 based on (a) summer solstice and (b) winter solstice of Qatar.

Table 3
Effect of the solar field size on the performance of S3 and S4 compared to the SRC with TES.

System	N_{hel}	At 50 MW power demand			25 MW power demand		
		η_{s-CO_2}	$\dot{m}_f$	$\dot{m}_{CO_2}$	η_{s-CO_2}	$\dot{m}_f$	$\dot{m}_{CO_2}$
		%	kg/s	kg/s	%	kg/s	kg/s
SRC with TES	4946	35.70	–	536	29.40	–	341
S3	4946	37.55	0.827	465	31.73	0.305	196
	2473	51.35	1.352	436	40.72	0.680	222
S4	4946	45.05	0.805	136	37.62	0.403	68
	2473	53.84	1.62	274	41.08	0.810	137

smaller solar field size with DOC works as the backbone of the energy source.

4.3. Off-design analysis of the power cycle blocks

Fig. 10 shows the effect of the compressor inlet temperature (CIT) and turbine inlet temperature (TIT) on the cycle efficiency and consumed fuel (natural gas) in S3 and S4 configurations. The increase of the CIT is imposed by the increase of the ambient temperature which is the sink of the dry cooling process. Therefore, as the ambient temperature increase the inlet temperature at the compressor inlet also increases which increases the compression power and reduces the cycle efficiency (by 8% for configurations). Also, the increase of the CIT also yields higher temperature at the inlet of the combustor which reduces the amount of the consumed fuel by 5.8% over the range of the CIT. But the increase of the compression power is more dominant than the decrease of the consumed fuel which eventually reduces the overall cycle efficiency. In contrasts, the increase of the TIT (which is achievable with higher fuel consumption but with about 15.8% lower than the stand-alone DOC sCO_2 power cycle) improves the cycle efficiency by 8.6% in S4 and 8.13% in S3. As the TIT increases from 550 °C to 750 °C, the fuel consumption is increased by about 57% in both configurations. It should be emphasized that S3, and S4 are able to capture the excess sCO_2 to transport it in proper conditions for commercial applications). Therefore, the efficiency improvement achieved at TIT of 750 °C (8.6% increase) increases the potential of integrating SPT and DOC system for the following reasons: (1) higher turbine inlet temperatures are achieved with lower fuel consumption than that in standard DOC system (by about 15.8%), (2) the produced power can be controlled and adjusted for the variation of the ambient conditions and power demand profiles without TES, (3) the capacity of the system can be scaled up by increasing the load of the combustor without any modification on the solar field components.

4.4. Effect of ambient temperature

The performance of the proposed configurations strongly depends on the ambient temperature that varies between day and night time as well as seasonally. This effect is shown by Fig. 11 (a)-(e) for S3 configuration (similar behavior is noted for S4). The ambient temperatures were selected based on sever and average summer and winter conditions in Qatar. Comparing Fig. 11 (a), (b), (c), and (d), it shows that as T_{am} increases, the mass flow rate across the receiver and the absorbed heat by the receiver are increased too (for instance, at winter T_{am} = 2 °C, (with $Q_{rec,in}$ = 320 MW and $T_{rec,in}$ = 378 °C), the m_{rec} = 400 kg/s, while at summer T_{am} = 45 °C, the m_{rec} increases to 749 kg/s) This implies that about 8.11 kg/s is increase in m_{rec} occurs for each degree increase in T_{am} which

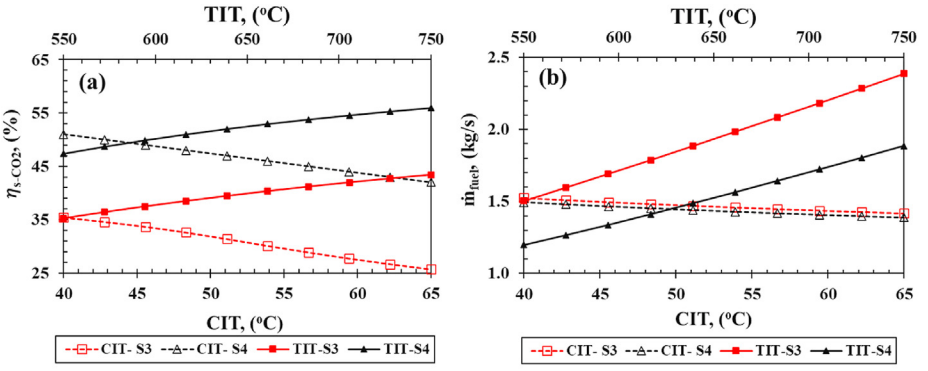

Fig. 10. Effect of (a) CIT, and (b) TIT on the cycle efficiency and consumed fuel in S3 and S4 configurations.

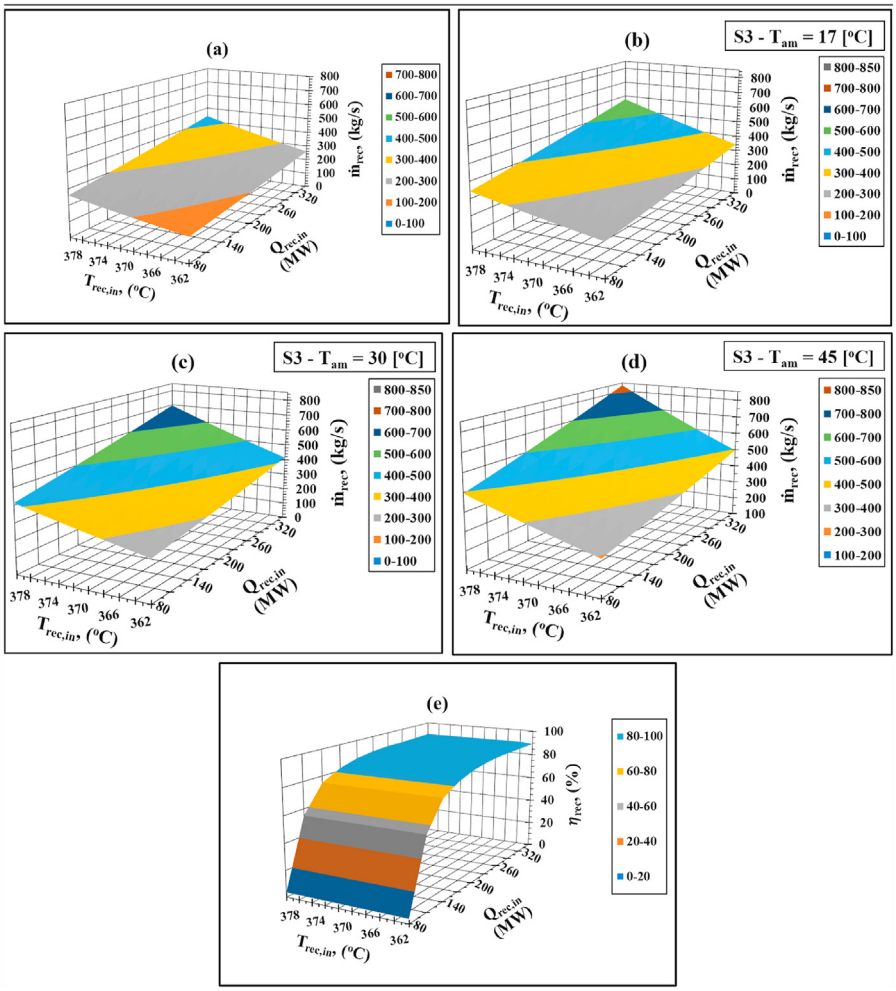

Fig. 11. Effect of the ambient temperature on the performance of the solar receiver of S3.

enhances the efficiency of the CSP system by the reduction of the receiver heat losses via convection and radiation with the ambient. However, this imposes more work on the compressor as the increase of the ambient temperature raises the temperature at the inlet of the compressor. Therefore, a slight decrease in the overall efficiency of the cycle is occurs at extremely high ambient temperature. On the other hand, extremely low ambient temperature negatively affect the performance of the receiver by enhancing the heat losses to the ambient.

5. Conclusions

This study investigates the off-design performance of two novel power cycle configurations that integrates the solar power tower (SPT) system with the direct oxy-combusted (DOC) intercooled sCO_2 power cycle. The analyzed configurations in this study were selected among five configurations and referred to as S3 and S4. In S3, the SPT system works as a preheater for the DOC system while in S4 the SPT system works as a reheater for the outlet flow of a high-pressure turbine. The off-design analysis approach first verified and validated against published results introduced by Yang. et al. [42] and the results shows good agreement with error less than 1%. Their cycle was a SPT with TES integrated with simple recuperated sCO_2 power cycle (Referred to as "Ref." in this study). Then, the off-design analysis of S3 and S3 is performed based on real ambient conditions and power demand profiles for two typical days in Qatar. Then, off-design operating conditions were applied by changing the compressor inlet temperature (CIT) and the turbine inlet temperature (TIT) to analyze their effects on the cycle efficiency and the fuel consumption. The main conclusions of the present study are:

- The design and off-design overall cycle efficiencies of S3 and S4 are higher than the conventional SPT-sCO_2 power systems. Compared to the Ref. Cycle, the cycle efficiency of S4 and S3 are higher by 15% and 7%, respectively, at the maximum power demand profile (which are close to the data used for the Ref. cycle).
- In S3 and S4, the solar field size can be reduced by 50% compared to the conventional SPT-sCO_2 systems with higher efficient operation as the DOC forms the backbone of the energy source.
- Although the efficiency of S4 is considerably higher than S3, S3 show better flexibility with the variation of the power demand. At 76% of the full load, the cycle efficiency is reduced by 5.64% in S4 and by 4.35% in S3.
- At the design point conditions, the increase of the CIT reduces the cycle efficiency (by 8%) but also reduces the amount of the consumed fuel (by 15.8%). On the other hand, the increase of the TIT improves the cycle efficiency (by 8.6%) but also increases the consumed fuel by (57%).
- From the overall analyses, it is recommended to design a combined SPT and DOC system with S4 configuration and the solar

field size is selected to cover the minimum power demand to achieve efficient and economic power block system.
- More control strategies need to be investigated and compares with the applied strategy in this study to mitigate the decrease of the cycle efficiency as the demand moves far from the full-design capacity.

CRediT authorship contribution statement

Ahmad K. Sleiti: Conceptualization, Investigation, Writing – original draft, Writing – review & editing, Resources, Formal analysis, Project administration, Funding acquisition, Supervision. **Wahib A. Al-Ammari:** Conceptualization, Writing – original draft, Investigation, Software, Data curation, Validation, Formal analysis.

Declaration of competing interest

The authors declare that they have no known competing financial interests or personal relationships that could have appeared to influence the work reported in this paper.

Acknowledgement

The work presented in this publication was made possible by NPRP-S grant # [11S-1231-170155] from the Qatar National Research Fund (a member of Qatar Foundation). The findings herein reflect the work, and are solely the responsibility, of the authors. Open Access funding provided by the Qatar National Library.

Appendix

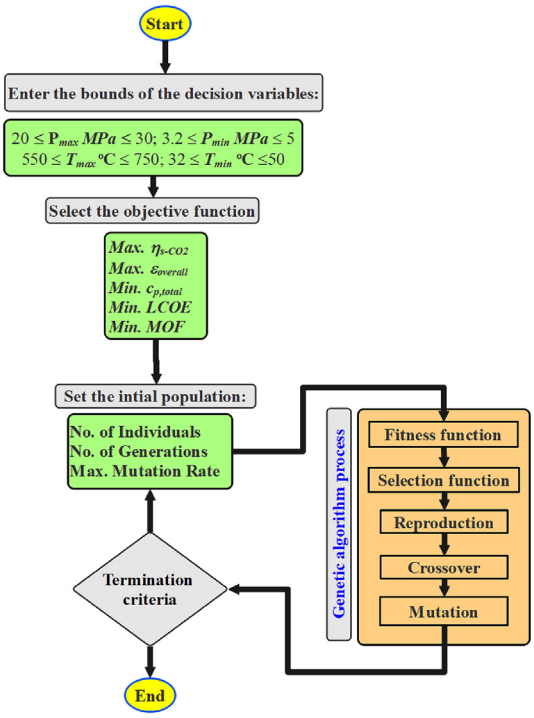

Fig. A2. The optimization methodology for the investigated SPT-DOC sCO_2 power cycles. Note: $\eta_{s\text{-}CO2}$ = overall cycle efficiency, $\varepsilon_{overall}$ = overall exergy efficiency of the system, $c_{p,total}$ = total product unit cost, LCOE = levelized cost of electricity, MOF = multi-objective function, Min. = minimize, and Max. = maximize.

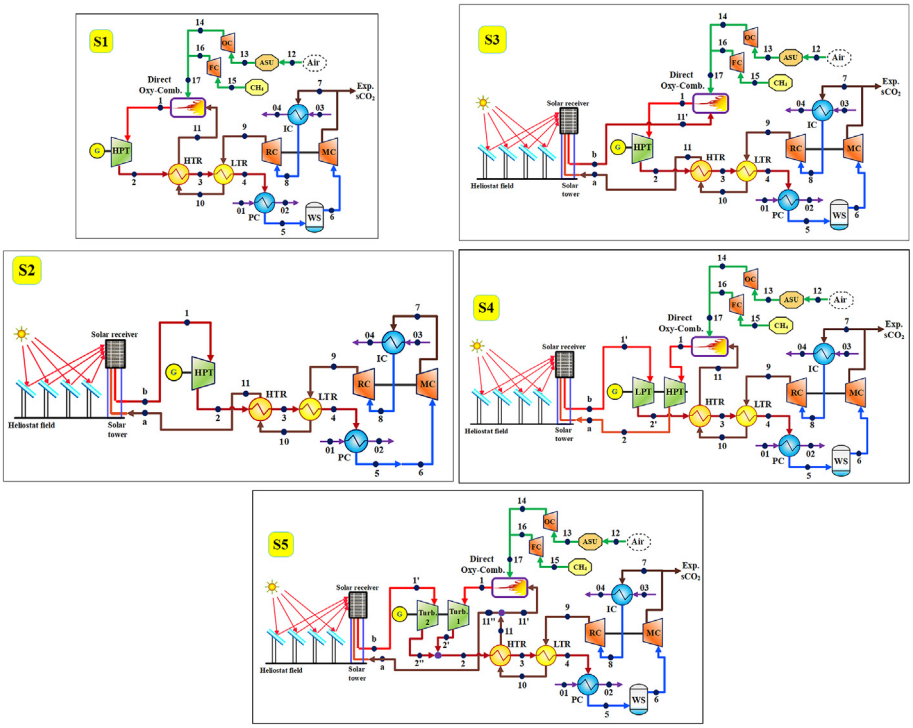

Fig. A1. Investigated configurations for the integration between the SPT and intercooled DOC sCO_2 power cycle.

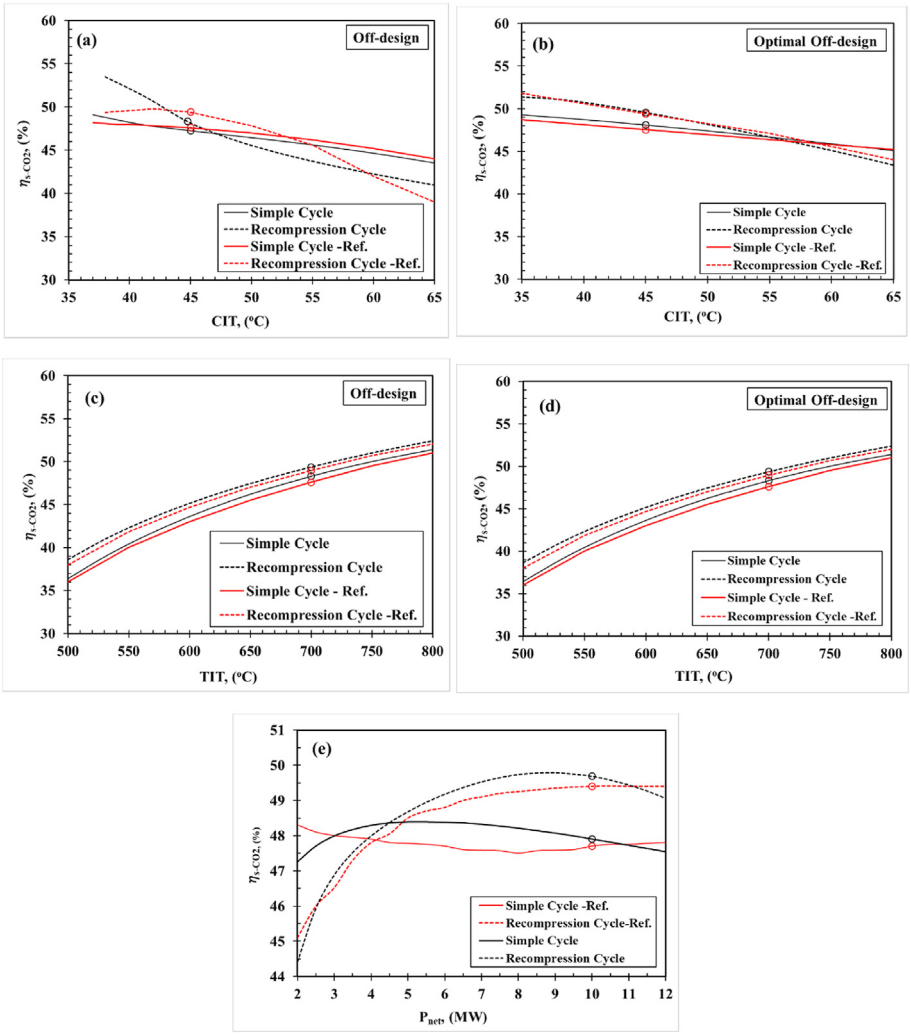

Fig. A3. Comparison between published results by Dyreby et al. [37] and those obtained by the model of the present study for the SRC and recompression sCO_2 power cycles with the off-design and optimal off-design of the CIT (a, b), TIT (c, d) and part-load operation (e). Note (1): Off-design = without adjusting the control variables and the output power is varied, Optimal off-design = the control variables are adjusted such that the output power remains constant at 10 MW. The control variables include the compressor inlet pressure and the main shaft speed (for both cycles) and the recompression fraction (for the recompression cycle only). Note (2): The results presented by Dyreby et al. [37] were based on experimental-based model using data being developed for use in a sCO_2 power cycle at the Sandia National Laboratory [37].

References

[1] J.M. Yin, Q.Y. Zheng, Z.R. Peng, X.R. Zhang, Review of supercritical CO2 power cycles integrated with CSP, Int. J. Energy Res. 44 (2020) 1337–1369, https://doi.org/10.1002/er.4909.

[2] O. Achkari, A. El Fadar, Latest developments on TES and CSP technologies – energy and environmental issues, applications and research trends, Appl. Therm. Eng. 167 (2020), 114806, https://doi.org/10.1016/j.applthermaleng.2019.114806.

[3] F. Alnaimat, Y. Rashid, Thermal energy storage in solar power plants: a review of the materials, associated limitations, and proposed solutions, Energies 12 (2019), https://doi.org/10.3390/en12214164.

[4] C. Liu, Z. Rao, Challenges in various thermal energy storage technologies, Sci. Bull. 62 (2017) 231–233, https://doi.org/10.1016/j.scib.2017.01.019.

[5] A.A. Khosa, T. Xu, B.Q. Xia, J. Yan, C.Y. Zhao, Technological challenges and industrial applications of CaCO3/CaO based thermal energy storage system – a review, Sol. Energy 193 (2019) 618–636, https://doi.org/10.1016/j.solener.2019.10.003.

[6] J.I. Linares, M.J. Montes, A. Cantizano, C. Sánchez, A novel supercritical CO2 recompression Brayton power cycle for power tower concentrating solar plants, Appl. Energy 263 (2020), 114644, https://doi.org/10.1016/j.apenergy.2020.114644.

[7] S. Son, J.Y. Heo, N. Il Kim, A. Jamal, J.I. Lee, Reduction of CO2 emission for solar power backup by direct integration of oxy-combustion supercritical CO2 power cycle with concentrated solar power, Energy Convers. Manag. 201 (2019), 112161, https://doi.org/10.1016/j.enconman.2019.112161.

[8] Y. Ma, T. Morosuk, J. Luo, M. Liu, J. Liu, Superstructure design and optimization on supercritical carbon dioxide cycle for application in concentrated solar power plant, Energy Convers. Manag. 206 (2020), 112290, https://doi.org/10.1016/j.enconman.2019.112290.

[9] A.G. Fernández, L.F. Cabeza, Corrosion monitoring and mitigation techniques on advanced thermal energy storage materials for CSP plants, Sol. Energy Mater. Sol. Cells 192 (2019) 179–187, https://doi.org/10.1016/j.solmat.2018.12.028.

[10] A. Palacios, M. Elena Navarro, C. Barreneche, Y. Ding, Hybrid 3 in 1 thermal energy storage system – outlook for a novel storage strategy, Appl. Energy 274 (2020), 115024, https://doi.org/10.1016/j.apenergy.2020.115024.

[11] C. Xu, T. Xin, X. Li, S. Li, Y. Sun, W. Liu, Y. Yang, A thermodynamic analysis of a solar hybrid coal-based direct-fired supercritical carbon dioxide power cycle, Energy Convers. Manag. 196 (2019) 77–91, https://doi.org/10.1016/j.enconman.2019.06.002.

[12] K. Wang, Y.L. He, Thermodynamic analysis and optimization of a molten salt solar power tower integrated with a recompression supercritical CO2 Brayton cycle based on integrated modeling, Energy Convers. Manag. 135 (2017) 336–350, https://doi.org/10.1016/j.enconman.2016.12.085.

[13] H. Liu, R. Zhai, K. Patchigolla, P. Turner, Y. Yang, Off-design thermodynamic performances of a combined solar tower and parabolic trough aided coal-fired power plant, Appl. Therm. Eng. 183 (2021), 116199, https://doi.org/10.1016/j.applthermaleng.2020.116199.

[14] M.R. Rodríguez-Sánchez, A. Sánchez-González, P.A. González-Gómez, C. Marugán-Cruz, D. Santana, Thermodynamic and economic assessment of a new generation of subcritical and supercritical solar power towers, Energy 118 (2017) 534–544, https://doi.org/10.1016/j.energy.2016.10.079.

[15] B.D. Iverson, T.M. Conboy, J.J. Pasch, A.M. Kruizenga, Supercritical CO2 Brayton cycles for solar-thermal energy, Appl. Energy 111 (2013) 957–970, https://

doi.org/10.1016/j.apenergy.2013.06.020.
[16] Y. Ma, X. Zhang, M. Liu, J. Yan, J. Liu, Proposal and assessment of a novel supercritical CO2 Brayton cycle integrated with LiBr absorption chiller for concentrated solar power applications, Energy 148 (2018) 839–854, https://doi.org/10.1016/j.energy.2018.01.155.
[17] H.H. Zhu, K. Wang, Y.L. He, Thermodynamic analysis and comparison for different direct-heated supercritical CO2 Brayton cycles integrated into a solar thermal power tower system, Energy 140 (2017) 144–157, https://doi.org/10.1016/j.energy.2017.08.067.
[18] J.Q. Guo, M.J. Li, J.L. Xu, J.J. Yan, K. Wang, Thermodynamic performance analysis of different supercritical Brayton cycles using CO2-based binary mixtures in the molten salt solar power tower systems, Energy 173 (2019) 785–798, https://doi.org/10.1016/j.energy.2019.02.008.
[19] M.T. White, G. Bianchi, L. Chai, S.A. Tassou, A.I. Sayma, Review of supercritical CO2 technologies and systems for power generation, Appl. Therm. Eng. 185 (2021), 116447, https://doi.org/10.1016/j.applthermaleng.2020.116447.
[20] X. Xu, K. Vignarooban, B. Xu, K. Hsu, A.M. Kannan, Prospects and problems of concentrating solar power technologies for power generation in the desert regions, Renew. Sustain. Energy Rev. 53 (2016) 1106–1131, https://doi.org/10.1016/j.rser.2015.09.015.
[21] F. Crespi, G. Gavagnin, D. Sánchez, G.S. Martínez, Supercritical carbon dioxide cycles for power generation: a review, Appl. Energy 195 (2017) 152–183, https://doi.org/10.1016/j.apenergy.2017.02.048.
[22] P. Wu, Y. Ma, C. Gao, W. Liu, J. Shan, Y. Huang, J. Wang, D. Zhang, X. Ran, A review of research and development of supercritical carbon dioxide Brayton cycle technology in nuclear engineering applications, Nucl. Eng. Des. 368 (2020), 110767, https://doi.org/10.1016/j.nucengdes.2020.110767.
[23] Y. Liu, Y. Wang, D. Huang, Supercritical CO2 Brayton cycle: a state-of-the-art review, Energy 189 (2019), 115900, https://doi.org/10.1016/j.energy.2019.115900.
[24] A.K. Sleiti, W.A. Al-Ammari, Energy and exergy analyses of novel supercritical CO2 Brayton cycles driven by direct oxy-fuel combustor, Fuel 294 (2021), 120557, https://doi.org/10.1016/j.fuel.2021.120557.
[25] A.K. Sleiti, W. Al-ammari, S. Ahmed, J. Kapat, Direct-fired oxy-combustion supercritical-CO2 power cycle with novel preheating configurations -thermodynamic and exergoeconomic analyses, Energy 226 (2021), 120441, https://doi.org/10.1016/j.energy.2021.120441.
[26] Y. Ma, T. Morozyuk, M. Liu, J. Yan, J. Liu, Optimal integration of recompression supercritical CO2 Brayton cycle with main compression intercooling in solar power tower system based on exergoeconomic approach, Appl. Energy 242 (2019) 1134–1154, https://doi.org/10.1016/j.apenergy.2019.03.155.
[27] M. Saeed, M.H. Kim, Analysis of a recompression supercritical carbon dioxide power cycle with an integrated turbine design/optimization algorithm, Energy 165 (2018) 93–111, https://doi.org/10.1016/j.energy.2018.09.058.
[28] Y. Sun, S. Duniam, Z. Guan, H. Gurgenci, P. Dong, J. Wang, K. Hooman, Coupling supercritical carbon dioxide Brayton cycle with spray-assisted dry cooling technology for concentrated solar power, Appl. Energy 251 (2019), 113328, https://doi.org/10.1016/j.apenergy.2019.113328.
[29] J.Q. Guo, M.J. Lia, J.L. Xu, Performance comparison of SPT systems integrated with various supercritical CO2-based mixture Brayton cycles based on multi-objective optimization, Energy Procedia 158 (2019) 1823–1828, https://doi.org/10.1016/j.egypro.2019.01.427.
[30] M. Abid, M.S. Khan, T.A.H. Ratlamwala, Comparative energy, exergy and exergo-economic analysis of solar driven supercritical carbon dioxide power and hydrogen generation cycle, Int. J. Hydrogen Energy 45 (2020) 5653–5667, https://doi.org/10.1016/j.ijhydene.2019.06.103.
[31] M. Atif, F.A. Al-Sulaiman, Energy and exergy analyses of solar tower power plant driven supercritical carbon dioxide recompression cycles for six different locations, Renew. Sustain. Energy Rev. 68 (2017) 153–167, https://doi.org/10.1016/j.rser.2016.09.122.
[32] T. Neises, C. Turchi, Supercritical carbon dioxide power cycle design and configuration optimization to minimize levelized cost of energy of molten salt power towers operating at 650 °C, Sol. Energy 181 (2019) 27–36, https://doi.org/10.1016/j.solener.2019.01.078.
[33] M. Liu, X. Zhang, K. Yang, Y. Ma, J. Yan, Optimization and comparison on supercritical CO2 power cycles integrated within coal-fired power plants considering the hot and cold end characteristics, Energy Convers. Manag. 195 (2019) 854–865, https://doi.org/10.1016/j.enconman.2019.05.077.
[34] A. de la Calle, A. Bayon, J. Pye, Techno-economic assessment of a high-efficiency, low-cost solar-thermal power system with sodium receiver, phase-change material storage, and supercritical CO2 recompression Brayton cycle, Sol. Energy 199 (2020) 885–900, https://doi.org/10.1016/j.solener.2020.01.004.
[35] Z. Ma, M.J. Li, K.M. Zhang, F. Yuan, Novel designs of hybrid thermal energy storage system and operation strategies for concentrated solar power plant, Energy 216 (2021), 119281, https://doi.org/10.1016/j.energy.2020.119281.
[36] I. Khamlich, K. Zeng, G. Flamant, J. Baeyens, C. Zou, J. Li, X. Yang, X. He, Q. Liu, H. Yang, Q. Yang, H. Chen, Technical and economic assessment of thermal energy storage in concentrated solar power plants within a spot electricity market, Renew. Sustain. Energy Rev. 139 (2021), 110583, https://doi.org/10.1016/j.rser.2020.110583.
[37] J.J. Dyreby, S.A. Klein, G.F. Nellis, D.T. Reindl, Modeling off-design and part-load performance of supercritical carbon dioxide power cycles, Proc. ASME Turbo Expo 8 (2013) 1–7, https://doi.org/10.1115/GT2013-95824.
[38] J.J. Dyreby, S.A. Klein, G.F. Nellis, D.T. Reindl, Development of advanced off-design models for supercritical carbon dioxide power cycles, Int. Congr. Adv. Nucl. Power Plants 4 (2012) (2012) 2711–2718. ICAPP 2012.
[39] S.A. Wright, C.S. Davidson, C. Husa, Off-design performance modeling results for a supercritical CO 2 waste heat recovery power system, 6th Int. Supercrit. CO2 Power Cycles Symp. (2018) 1–10.
[40] S. Duniam, A. Veeraragavan, Off-design performance of the supercritical carbon dioxide recompression Brayton cycle with NDDCT cooling for concentrating solar power, Energy 187 (2019), 115992, https://doi.org/10.1016/j.energy.2019.115992.
[41] T. Neises, Steady-state off-design modeling of the supercritical carbon dioxide recompression cycle for concentrating solar power applications with two-tank sensible-heat storage, Sol. Energy 212 (2020) 19–33, https://doi.org/10.1016/j.solener.2020.10.041.
[42] J. Yang, Z. Yang, Y. Duan, Off-design performance of a supercritical CO2 Brayton cycle integrated with a solar power tower system, Energy 201 (2020), 117676, https://doi.org/10.1016/j.energy.2020.117676.
[43] R. Chen, M. Romero, J. González-Aguilar, F. Rovense, Z. Rao, S. Liao, Design and off-design performance comparison of supercritical carbon dioxide Brayton cycles for particle-based high temperature concentrating solar power plants, Energy Convers. Manag. 232 (2021), https://doi.org/10.1016/j.enconman.2021.113870.
[44] X. Wang, X. Li, Q. Li, L. Liu, C. Liu, Performance of a solar thermal power plant with direct air-cooled supercritical carbon dioxide Brayton cycle under off-design conditions, Appl. Energy 261 (2020), 114359, https://doi.org/10.1016/j.apenergy.2019.114359.
[45] H. Li, G. Fan, L. Cao, Y. Yang, X. Yan, Y. Dai, G. Zhang, J. Wang, A comprehensive investigation on the design and off-design performance of supercritical carbon dioxide power system based on the small-scale lead-cooled fast reactor, J. Clean. Prod. 256 (2020), 120720, https://doi.org/10.1016/j.jclepro.2020.120720.
[46] G. Fan, H. Li, Y. Du, K. Chen, S. Zheng, Y. Dai, Preliminary design and part-load performance analysis of a recompression supercritical carbon dioxide cycle combined with a transcritical carbon dioxide cycle, Energy Convers. Manag. 212 (2020), 112758, https://doi.org/10.1016/j.enconman.2020.112758.
[47] B. Li, S. Wang, Y. Xu, L. Song, Study on the off-design performance of supercritical carbon dioxide power cycle for waste heat recovery of gas turbine, Energy Convers. Manag. 233 (2021), 113890, https://doi.org/10.1016/j.enconman.2021.113890.
[48] Y. Tong, L. Duan, L. Pang, Off-design performance analysis of a new 300 MW supercritical CO2 coal-fired boiler, Energy 216 (2021), https://doi.org/10.1016/j.energy.2020.119306.
[49] D. Sánchez, R. Chacartegui, J.M. Muñoz De Escalona, A. Muñoz, T. Sánchez, Performance analysis of a MCFC & supercritical carbon dioxide hybrid cycle under part load operation, Int. J. Hydrogen Energy 36 (2011) 10327–10336, https://doi.org/10.1016/j.ijhydene.2010.09.072.
[50] A.K. Sleiti, W.A. Al-Ammaria, M. Al-Khawaja, A novel solar integrated distillation and cooling system - design and analysis, Sol. Energy 206 (2020) 68–83, https://doi.org/10.1016/j.solener.2020.05.107.
[51] A.K. Sleiti, W.A. Al-Ammari, M. Al-Khawaja, Integrated novel solar distillation and solar single-effect absorption systems, Desalination 507 (2021), 115032, https://doi.org/10.1016/j.desal.2021.115032.
[52] W. Chan, X. Lei, F. Chang, H. Li, Thermodynamic analysis and optimization of Allam cycle with a reheating configuration, Energy Convers. Manag. 224 (2020), 113382, https://doi.org/10.1016/j.enconman.2020.113382.
[53] K. Wang, Y.L. He, H.H. Zhu, Integration between supercritical CO2 Brayton cycles and molten salt solar power towers: a review and a comprehensive comparison of different cycle layouts, Appl. Energy 195 (2017) 819–836, https://doi.org/10.1016/j.apenergy.2017.03.099.
[54] N. Zhang, N. Lior, M. Liu, W. Han, COOLCEP (cool clean efficient power): a novel CO2-capturing oxy-fuel power system with LNG (liquefied natural gas) coldness energy utilization, Energy 35 (2010) 1200–1210, https://doi.org/10.1016/j.energy.2009.04.002.
[55] R. Scaccabarozzi, M. Gatti, E. Martelli, Thermodynamic analysis and numerical optimization of the NET Power oxy-combustion cycle, Appl. Energy 178 (2016) 505–526, https://doi.org/10.1016/j.apenergy.2016.06.060.
[56] A. Rogalev, E. Grigoriev, V. Kindra, N. Rogalev, Thermodynamic optimization and equipment development for a high efficient fossil fuel power plant with zero emissions, J. Clean. Prod. 236 (2019), 117592, https://doi.org/10.1016/j.jclepro.2019.07.067.
[57] C.S. Turchi, Z. Ma, T.W. Neises, M.J. Wagner, Thermodynamic study of advanced supercritical carbon dioxide power cycles for concentrating solar power systems, J. Sol. Energy Eng. Trans. ASME 135 (2013) 1–7, https://doi.org/10.1115/1.4024030.
[58] İ.Ş. Bayram, M. Koç, Demand side management for peak reduction and PV integration in Qatar, Proc. 2017 IEEE 14th Int. Conf. Netw., Sens. Control. ICNSC (2017) (2017) 251–256, https://doi.org/10.1109/ICNSC.2017.8000100.
[59] F. Touati, M.A. Al-Hitmi, N.A. Chowdhury, J.A. Hamad, A.J.R. San Pedro Gonzales, Investigation of solar PV performance under Doha weather using a customized measurement and monitoring system, Renew. Energy 89 (2016) 564–577, https://doi.org/10.1016/j.renene.2015.12.046.